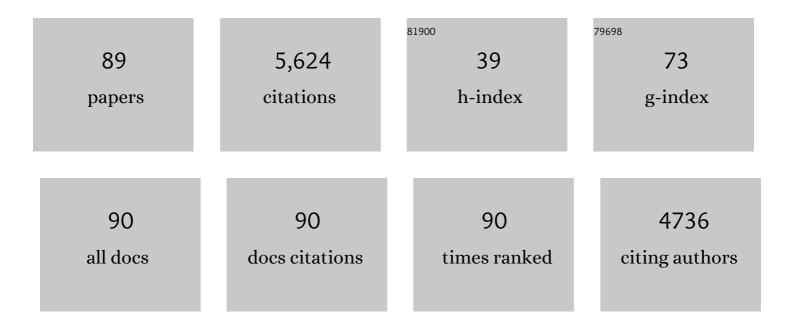
## Andrew J Burghardt

List of Publications by Year in descending order

Source: https://exaly.com/author-pdf/5431508/publications.pdf Version: 2024-02-01



#	Article	IF	CITATIONS
1	High-Resolution Peripheral Quantitative Computed Tomographic Imaging of Cortical and Trabecular Bone Microarchitecture in Patients with Type 2 Diabetes Mellitus. Journal of Clinical Endocrinology and Metabolism, 2010, 95, 5045-5055.	3.6	407
2	Reproducibility of direct quantitative measures of cortical bone microarchitecture of the distal radius and tibia by HR-pQCT. Bone, 2010, 47, 519-528.	2.9	397
3	Increased cortical porosity in type 2 diabetic postmenopausal women with fragility fractures. Journal of Bone and Mineral Research, 2013, 28, 313-324.	2.8	369
4	Age- and gender-related differences in the geometric properties and biomechanical significance of intracortical porosity in the distal radius and tibia. Journal of Bone and Mineral Research, 2010, 25, 983-993.	2.8	271
5	Visual grading of motion induced image degradation in high resolution peripheral computed tomography: Impact of image quality on measures of bone density and micro-architecture. Bone, 2012, 50, 111-118.	2.9	223
6	High-resolution Computed Tomography for Clinical Imaging of Bone Microarchitecture. Clinical Orthopaedics and Related Research, 2011, 469, 2179-2193.	1.5	213
7	A longitudinal HR-pQCT study of alendronate treatment in postmenopausal women with low bone density: Relations among density, cortical and trabecular microarchitecture, biomechanics, and bone turnover. Journal of Bone and Mineral Research, 2010, 25, 2558-2571.	2.8	210
8	Does vertebral bone marrow fat content correlate with abdominal adipose tissue, lumbar spine bone mineral density, and blood biomarkers in women with type 2 diabetes mellitus?. Journal of Magnetic Resonance Imaging, 2012, 35, 117-124.	3.4	196
9	High-Resolution Peripheral Quantitative Computed Tomography for the Assessment of Bone Strength and Structure: A Review by the Canadian Bone Strength Working Group. Current Osteoporosis Reports, 2013, 11, 136-146.	3.6	182
10	High-Resolution Imaging Techniques for the Assessment of Osteoporosis. Radiologic Clinics of North America, 2010, 48, 601-621.	1.8	174
11	In Vivo Determination of Bone Structure in Postmenopausal Women: A Comparison of HR-pQCT and High-Field MR Imaging. Journal of Bone and Mineral Research, 2008, 23, 463-474.	2.8	122
12	Morphology of the human vertebral endplate. Journal of Orthopaedic Research, 2012, 30, 280-287.	2.3	121
13	Serum miRNA Signatures Are Indicative of Skeletal Fractures in Postmenopausal Women With and Without Type 2 Diabetes and Influence Osteogenic and Adipogenic Differentiation of Adipose Tissue–Derived Mesenchymal Stem Cells In Vitro. Journal of Bone and Mineral Research, 2016, 31, 2173-2192.	2.8	115
14	A Local Adaptive Threshold Strategy for High Resolution Peripheral Quantitative Computed Tomography of Trabecular Bone. Annals of Biomedical Engineering, 2007, 35, 1678-1686.	2.5	104
15	Multicenter precision of cortical and trabecular bone quality measures assessed by high-resolution peripheral quantitative computed tomography. Journal of Bone and Mineral Research, 2013, 28, 524-536.	2.8	98
16	The effect of voxel size on highâ€resolution peripheral computed tomography measurements of trabecular and cortical bone microstructure. Medical Physics, 2012, 39, 1893-1903.	3.0	96
17	HRâ€pQCT Measures of Bone Microarchitecture Predict Fracture: Systematic Review and Metaâ€Analysis. Journal of Bone and Mineral Research, 2020, 35, 446-459.	2.8	92
18	Human Disc Nucleus Properties and Vertebral Endplate Permeability. Spine, 2011, 36, 512-520.	2.0	90

ANDREW J BURGHARDT

#	Article	IF	CITATIONS
19	Quantitative Assessment of Bone Tissue Mineralization with Polychromatic Micro-Computed Tomography. Calcified Tissue International, 2008, 83, 129-138.	3.1	89
20	Quantitative characterization of subject motion in HR-pQCT images of the distal radius and tibia. Bone, 2011, 48, 1291-1297.	2.9	88
21	Microarchitecture and Peripheral BMD are Impaired in Postmenopausal White Women With Fracture Independently of Total Hip <i>T</i> -Score: An International Multicenter Study. Journal of Bone and Mineral Research, 2016, 31, 1158-1166.	2.8	69
22	Resolution Dependence of the Non-metric Trabecular Structure Indices. Bone, 2008, 42, 728-736.	2.9	67
23	Regional variations of gender-specific and age-related differences in trabecular bone structure of the distal radius and tibia. Bone, 2010, 46, 1652-1660.	2.9	66
24	The influence of disuse on bone microstructure and mechanics assessed by HR-pQCT. Bone, 2014, 63, 132-140.	2.9	66
25	Assessment of trabecular bone structure of the calcaneus using multi-detector CT: Correlation with microCT and biomechanical testing. Bone, 2009, 44, 976-983.	2.9	65
26	Validation of bone marrow fat quantification in the presence of trabecular bone using MRI. Journal of Magnetic Resonance Imaging, 2015, 42, 539-544.	3.4	65
27	In vivo ultraâ€highâ€field magnetic resonance imaging of trabecular bone microarchitecture at 7 T. Journal of Magnetic Resonance Imaging, 2008, 27, 854-859.	3.4	63
28	Quantitative In Vivo HR-pQCT Imaging of 3D Wrist and Metacarpophalangeal Joint Space Width in Rheumatoid Arthritis. Annals of Biomedical Engineering, 2013, 41, 2553-2564.	2.5	60
29	Volumetric Bone Mineral Density and Failure Load of Distal Limbs Predict Incident Clinical Fracture Independent of FRAX and Clinical Risk Factors Among Older Men. Journal of Bone and Mineral Research, 2018, 33, 1302-1311.	2.8	57
30	Noninvasive imaging of bone microarchitecture. Annals of the New York Academy of Sciences, 2011, 1240, 77-87.	3.8	56
31	Volumetric femoral BMD, bone geometry, and serum sclerostin levels differ between type 2 diabetic postmenopausal women with and without fragility fractures. Osteoporosis International, 2015, 26, 1283-1293.	3.1	54
32	Assessment of trabecular bone structure using MDCT: comparison of 64- and 320-slice CT using HR-pQCT as the reference standard. European Radiology, 2010, 20, 458-468.	4.5	52
33	Age- and gender-related differences in cortical geometry and microstructure: Improved sensitivity by regional analysis. Bone, 2013, 52, 623-631.	2.9	51
34	The Effects of Geometric and Threshold Definitions on Cortical Bone Metrics Assessed by In Vivo High-Resolution Peripheral Quantitative Computed Tomography. Calcified Tissue International, 2007, 81, 364-371.	3.1	50
35	Longitudinal evaluation of the effects of alendronate on MRI bone microarchitecture in postmenopausal osteopenic women. Bone, 2011, 48, 611-621.	2.9	47
36	Cortical bone laminar analysis reveals increased midcortical and periosteal porosity in type 2 diabetic postmenopausal women with history of fragility fractures compared to fracture-free diabetics. Osteoporosis International, 2016, 27, 2791-2802.	3.1	47

Andrew J Burghardt

#	Article	IF	CITATIONS
37	Variations in morphological and biomechanical indices at the distal radius in subjects with identical BMD. Journal of Biomechanics, 2011, 44, 257-266.	2.1	44
38	Accuracy of volumetric bone mineral density measurement in high-resolution peripheral quantitative computed tomography. Bone, 2009, 45, 473-479.	2.9	41
39	Quantitative and Semiquantitative Bone Erosion Assessment on High-resolution Peripheral Quantitative Computed Tomography in Rheumatoid Arthritis. Journal of Rheumatology, 2013, 40, 408-416.	2.0	41
40	Trabecular Bone Structure Analysis in the Osteoporotic Spine Using a Clinical In Vivo Setup for 64-Slice MDCT Imaging: Comparison to μCT Imaging and μFE Modeling. Journal of Bone and Mineral Research, 2009, 24, 1628-1637.	2.8	38
41	Higher doses of bisphosphonates further improve bone mass, architecture, and strength but not the tissue material properties in aged rats. Bone, 2010, 46, 1267-1274.	2.9	38
42	Spatial distribution of intracortical porosity varies across age and sex. Bone, 2015, 75, 88-95.	2.9	38
43	Kartogenin treatment prevented joint degeneration in a rodent model of osteoarthritis: A pilot study. Journal of Orthopaedic Research, 2016, 34, 1780-1789.	2.3	37
44	The comparability of HR-pQCT bone measurements is improved by scanning anatomically standardized regions. Osteoporosis International, 2017, 28, 2115-2128.	3.1	35
45	Sensitivity of damage predictions to tissue level yield properties and apparent loading conditions. Journal of Biomechanics, 2001, 34, 699-706.	2.1	34
46	Heterogeneity of bone microstructure in the femoral head in patients with osteoporosis: An ex vivo HR-pQCT study. Bone, 2013, 56, 139-146.	2.9	33
47	Correlation of structural abnormalities of the wrist and metacarpophalangeal joints evaluated by high-resolution peripheral quantitative computed tomography, 3ATesla magnetic resonance imaging and conventional radiographs in rheumatoid arthritis. International Journal of Rheumatic Diseases, 2015, 18, 628-639.	1.9	33
48	Operator variability in scan positioning is a major component of HR-pQCT precision error and is reduced by standardized training. Osteoporosis International, 2017, 28, 245-257.	3.1	33
49	High-Resolution Peripheral Quantitative Computed Tomography for Bone Evaluation in Inflammatory Rheumatic Disease. Frontiers in Medicine, 2020, 7, 337.	2.6	32
50	Contribution of the intra-specimen variations in tissue mineralization to PTH- and raloxifene-induced changes in stiffness of rat vertebrae. Bone, 2010, 46, 1162-1169.	2.9	29
51	Ultrashort echo time MRI of cortical bone at 7 tesla field strength: A feasibility study. Journal of Magnetic Resonance Imaging, 2011, 34, 691-695.	3.4	29
52	Structural analysis of cortical porosity applied to HR-pQCT data. Medical Physics, 2013, 41, 013701.	3.0	29
53	Evaluation of fetal bone structure and mineralization in IGF-I deficient mice using synchrotron radiation microtomography and Fourier transform infrared spectroscopy. Bone, 2007, 40, 160-168.	2.9	28
54	Postmenopausal women treated with combination parathyroid hormone (1–84) and ibandronate demonstrate different microstructural changes at the radius vs. tibia: the PTH and Ibandronate Combination Study (PICS). Osteoporosis International, 2013, 24, 2591-2601.	3.1	28

Andrew J Burghardt

#	Article	IF	CITATIONS
55	Three-dimensional analysis of subchondral cysts in hip osteoarthritis: An ex vivo HR-pQCT study. Bone, 2014, 66, 140-145.	2.9	28
56	Assessment of 3-month changes in bone microstructure under anti-TNFα therapy in patients with rheumatoid arthritis using high-resolution peripheral quantitative computed tomography (HR-pQCT). Arthritis Research and Therapy, 2017, 19, 222.	3.5	27
57	Quantifying sex, race, and age specific differences in bone microstructure requires measurement of anatomically equivalent regions. Bone, 2017, 101, 206-213.	2.9	26
58	Quantification of lower leg arterial calcifications by high-resolution peripheral quantitative computed tomography. Bone, 2014, 58, 42-47.	2.9	25
59	Computational identification and quantification of trabecular microarchitecture classes by 3-D texture analysis-based clustering. Bone, 2013, 54, 133-140.	2.9	23
60	Consensus approach for 3D joint space width of metacarpophalangeal joints of rheumatoid arthritis patients using high-resolution peripheral quantitative computed tomography. Quantitative Imaging in Medicine and Surgery, 2020, 10, 314-325.	2.0	23
61	Automatic multi-parametric quantification of the proximal femur with quantitative computed tomography. Quantitative Imaging in Medicine and Surgery, 2015, 5, 552-68.	2.0	23
62	Wavelet-based characterization of vertebral trabecular bone structure from magnetic resonance images at 3 T compared with micro-computed tomographic measurements. Magnetic Resonance Imaging, 2007, 25, 392-398.	1.8	22
63	Imaging longitudinal changes in articular cartilage and bone following doxycycline treatment in a rabbit anterior cruciate ligament transection model of osteoarthritis. Magnetic Resonance Imaging, 2012, 30, 271-282.	1.8	17
64	Quantitative characterization of metacarpal and radial bone in rheumatoid arthritis using high resolution- peripheral quantitative computed tomography. International Journal of Rheumatic Diseases, 2017, 20, 353-362.	1.9	16
65	Bone Structure and Perfusion Quantification of Bone Marrow Edema Pattern in the Wrist of Patients with Rheumatoid Arthritis: A Multimodality Study. Journal of Rheumatology, 2014, 41, 1766-1773.	2.0	14
66	Longitudinal Evolution of Bone Microarchitecture and Bone Strength in Type 2 Diabetic Postmenopausal Women With and Without History of Fragility Fractures—A 5-Year Follow-Up Study Using High Resolution Peripheral Quantitative Computed Tomography. Frontiers in Endocrinology, 2021, 12, 599316.	3.5	13
67	CT Muscle Density, D3Cr Muscle Mass, and Body Fat Associations With Physical Performance, Mobility Outcomes, and Mortality Risk in Older Men. Journals of Gerontology - Series A Biological Sciences and Medical Sciences, 2022, 77, 790-799.	3.6	13
68	Trabecular Reorganization in Consecutive Iliac Crest Biopsies when Switching from Bisphosphonate to Strontium Ranelate Treatment. PLoS ONE, 2011, 6, e23638.	2.5	12
69	Accelerated Bone Loss in Older Men: Effects on Bone Microarchitecture and Strength. Journal of Bone and Mineral Research, 2018, 33, 1859-1869.	2.8	12
70	Structural Changes over a Short Period Are Associated with Functional Assessments in Rheumatoid Arthritis. Journal of Rheumatology, 2019, 46, 676-684.	2.0	12
71	The SPECTRA Collaboration OMERACT Special Interest Group: Current Research and Future Directions. Journal of Rheumatology, 2017, 44, 1911-1915.	2.0	11
72	Hip Fracture Discrimination Based on Statistical Multi-parametric Modeling (SMPM). Annals of Biomedical Engineering, 2019, 47, 2199-2212.	2.5	11

#	Article	IF	CITATIONS
73	Determining Metacarpophalangeal Flexion Angle Tolerance for Reliable Volumetric Joint Space Measurements by High-resolution Peripheral Quantitative Computed Tomography. Journal of Rheumatology, 2016, 43, 1941-1944.	2.0	10
74	Novel anthropomorphic hip phantom corrects systemic interscanner differences in proximal femoral vBMD. Physics in Medicine and Biology, 2014, 59, 7819-7834.	3.0	9
75	Statistical Parametric Mapping of HR-pQCT Images: A Tool for Population-Based Local Comparisons of Micro-Scale Bone Features. Annals of Biomedical Engineering, 2017, 45, 949-962.	2.5	9
76	Biochemical Markers of Bone Turnover in Older Adults With Type 1 Diabetes. Journal of Clinical Endocrinology and Metabolism, 2022, 107, e2405-e2416.	3.6	9
77	Improved Trabecular Bone Structure of 20-Month-Old Male Spontaneously Hypertensive Rats. Calcified Tissue International, 2014, 95, 282-291.	3.1	8
78	Bone microstructure in men assessed by HR-pQCT: Associations with risk factors and differences between men with normal, low, and osteoporosis-range areal BMD. Bone Reports, 2016, 5, 312-319.	0.4	7
79	Reliability and Change in Erosion Measurements by High-resolution Peripheral Quantitative Computed Tomography in a Longitudinal Dataset of Rheumatoid Arthritis Patients. Journal of Rheumatology, 2021, 48, 348-351.	2.0	6
80	Objective measures of moderate to vigorous physical activity are associated with higher distal limb bone strength among elderly men. Bone, 2020, 132, 115198.	2.9	5
81	Differences in bone mineral density and morphometry measurements by fixed versus relative offset methods in high-resolution peripheral quantitative computed tomography. Bone, 2021, 149, 115973.	2.9	4
82	Interpretation of Bone Mineral Density Z-Scores by Dual-Energy X-Ray Absorptiometry in Transgender and Gender Diverse Youth Prior to Gender-Affirming Medical Therapy. Journal of Clinical Densitometry, 2022, 25, 559-568.	1.2	4
83	Vascular patterning and permeability in prostate cancer models with differing osteogenic properties. NMR in Biomedicine, 2012, 25, 843-851.	2.8	3
84	Super-resolution/segmentation of 3D trabecular bone images with total variation and nonconvex Cahn-Hilliard functional. , 2017, , .		3
85	High-Resolution Imaging Techniques for Bone Quality Assessment. , 2018, , 1007-1041.		3
86	High-Resolution Imaging Techniques for Bone Quality Assessment. , 2011, , 891-925.		1
87	Global and Spatial Compartmental Interrelationships of Bone Density, Microstructure, Geometry and Biomechanics in the Distal Radius in a Colles' Fracture Study Using HR-pQCT. Frontiers in Endocrinology, 2021, 12, 568454.	3.5	1
88	Augmenting Osteoporosis Imaging with Machine Learning. Current Osteoporosis Reports, 2021, 19, 699-709.	3.6	1
89	Semi-blind joint super-resolution/segmentation of 3D trabecular bone images by a TV box approach. , 2015, , .		Ο